The shape of dark matter halos in the AURIGA simulations

Jesus Prada,[1][*] Jaime E. Forero-Romero,[1] Volker Springel[2]

[1] *Departamento de Fśica, Universidad de los Andes, Cra. 1 No. 18A-10, Edificio Ip, Bogot; Colombia.*
[2] *Heidelberg Institute for Theoretical Studies, Schloss-Wolfsbrunnenweg 35, D-69118 Heidelberg Germany.*

ABSTRACT
We measure the shape of the dark matter halos of Milky Way type galaxies.

Key words: keyword1 – keyword2 – keyword3

1 INTRODUCTION

A robust prediction of the Cold Dark Matter (CDM) paradigm is that DM halos are ellipsoidal and can be characterized by the principal axes $a > b > c$. This ellipsoidal shape is mostly due to the anisotropical and clumpy accretion of matter influenced by environmental structures. Numerical studies how that the shape has a strong mass dependence (Allgood et al. 2006), halos are also rounder at the outerskirts than at the inner part. Shape also evolves with cosmic time, halos get rounder as they evolve.

There is however a high degree of uncertainty on what is the degree of uncertainty on the degree of ellipticity of the Milky Way DM halo. This problem has been addressed both by observations and simulations. The difficulty in making an observational measurement lies in the indirect nature of the effect; i.e. the ellipticity can only be constrained by its effects on quantities such as stellar radial velocities. In simulations the uncertainty on predicting the MW DM ellipticity is driven by the different physical effects that should be modeled and its different possible numerical implementations.

Observationally some studies prefer oblate (i.e. a=b>c) configurations at small distances around ≤ 20 kpc (see Law & Majewski 2010; Bovy et al. 2016; Loebman et al. 2012; Olling & Merrifield 2000; Banerjee & Jog 2011) and more triaxial and prolate configurations on the outter distances ≥ 20 kpc (see Vera-Ciro & Helmi 2013; Law et al. 2009; Deg & Widrow 2013; Banerjee & Jog 2011). However, some studies are inclined towards prolate configurations even at the inner parts of the halo (see Bowden et al. 2016), and although it previously seemed that a triaxial DM halo on the outerskirts would be necessary to fully explain the characterization of the Sagittarius stream (Law et al. 2009), recent studies questioned this claim by reporting inconsistencies with narrow stellar streams Pearson et al. (2015) or finding

that the relaxation of other constraints may make this claim unnecessary Ibata et al. (2013).

In simulations there is strong evidence claiming that the presence of baryons produces axisymmetrical halos. For instance, some studies have shown that the DM halo shape must be axisymmetrical to ensure the stability of a hydrodynamical disk embeded in a static DM halo. Other have studied this rounding effect by simulating the disk as rigid potential inside an N-body triaxial DM halo Debattista et al. (2008); Debattista et al. (2013); Kazantzidis et al. (2010) finding that the halo responds to the disk by becoming less triaxial.

The caveat of the studies mentioned above is that they do not follow baryons in the whole cosmological context. Other studies overcome this limitation by using resimulations (Abadi et al. 2010; Bryan et al. 2013) finding that the feeback related to star formation in the disk drives the strenght of the round effect. Recently Chua et al. (2018a) made a study in a cosmological simulation to compare the effect of including baryons. They do find, on average, rounder halo shapes once hydrodynamic effects are included, but it is uncertain the strenght of this statistical effect on galaxies similar to the MW.

All these difficulties (enough numerical resolution, explicit cosmological context, appropriate feedback physics to produce realistic MW disks) have limited the studies that want to study the rounding effect of baryons in MW-like galaxies. In this work we overcome all these limitations by analyzing the results of state-of-the-art hydrodynamical simulations of isolated halos that resemble the Milky Way. We also perform a convergence study with simulation performed at different resolution levels and explicitly compare the role of DM only vs. DM+hydro on the MW DM halo shape.

[*] E-mail: jd.prada1760@uniandes.edu.co

Reference	q_ρ	s_ρ	q_ϕ	s_ϕ	R	θ	comment
Olling & Merrifield (2000)	**1.00**	**0.80**			$\simeq 8$kpc	0°	Method: Stellar dynamics and HI density.
Law et al. (2009)			**0.83**	**0.67**	$\lesssim 60$kpc	90°	Mid-axis orientation. Method: Sagittarius stream
Law & Majewski (2010)			**0.99**	**0.72**	[20kpc,60kpc]	90°	Mid-axis orientation, Method: Sagittarius stream
Loebman et al. (2012)	**1.00**	**0.47**			~ 20kpc	0°	Method: SDSS statistics
Deg & Widrow (2013)	0.72	0.28	0.82	0.40	[20kpc,60kpc]	90°	Mid-axis orientation. Method: Sagittarius stream
Vera-Ciro & Helmi (2013)			**1.00**	**0.90**	$\lesssim 10$kpc	0°	Method: Sagittarius stream & LMC
			0.90	**0.80**	$\gtrsim 10$kpc	90°	Mid-axis orientation on the outside.
Bovy et al. (2016)	**0.95**	**0.95**			$\lesssim 20$kpc	90°	Method: Stellar streams
Bowden et al. (2016)			$[\mathbf{0.5, 0.66}]$	$[\mathbf{0.5, 0.66}]$	[5kpc,10kpc]	90°	Weak constraint on prolate halo. Method: SDSS stars dynamics.
Banerjee & Jog (2011)	**1**	**1**			9kpc	0°	Method: HI gas.
	0.5	**0.5**			24kpc	0°	Monotonical change between radial regimes.
Johnston et al. (2005)	**1**	$[\mathbf{0.83 - 0.92}]$			$\lesssim 60$kpc	0°	Method: Sagittarius stream

Table 1. (TODO: compute analogues in isopotential or isodensity according to Binney and Tremaine)

Reference	q_ρ	s_ρ	q_ϕ	s_ϕ	R	comment
Chua et al. (2018b)	$\mathbf{0.88 \pm 0.10}$	$\mathbf{0.70 \pm 0.11}$			$0.15 R_{200}$	Illustris
Bryan et al. (2013)	$[\mathbf{0.84, 0.86}]$	$[\mathbf{0.66, 0.70}]$			R_{200}	For different cosmologies and feedback recipies. Calculated from a fit at $M_\odot = 10^12$
Abadi et al. (2010)			**0.98**	**0.85**	-	Almost independent of radius. No feedback: boundary case

Table 2. (TODO: compute analogues in isopotential or isodensity according to Binney and Tremaine)

2 NUMERICAL SIMULATIONS

In this work we use the results of the state-of-the art Auriga simulations (Grand et al. 2017). The objects in those simulations were selected from a set of 30 isolated halos in the Evolution and Assembly of GaLaxies and their Environments (EAGLE) project (Schaye et al. 2015). These halos were randomly selected from a sample of the most isolated halos whose virial mass M_{200} varied between $10^{12} M_\odot$ and $2 \times 10^{12} M_\odot$. These halos were re-simulated with higher resolution an varying physical realism using the AREPO code (Springel 2010).

All 30 halos were simulated within resolution defined for Aquarius simulations corresponding to $\sim 3 \times 10^6$ high resolution DM particles of $\sim 2.5 \times 10^5 M_\odot$. This resolution is labeled as Level 4, the main details for each halo are consigned in Table 3. From these 30 halos, 6 of them where re-simulated at higher resolution (labeled as Level 3) taking into account a spatial factor of 2 in each dimension. Details of Level 3 halos are in Table 4. Furthermore, for each halo in each level of resolution there are two versions of the simulation: DM-only and DM plus baryons with magneto-hydrodynamical (MHD) physics.

3 DETERMINING THE HALO SHAPE

The DM halo shape at a fixed radius is an estimate of either the isopotential or isodensity surfaces. Observational inference models usually estimate the isopotential contours which are probed by tracers (gas, stars), while simulations work with the isodensity contours which can be directly calculated from particle positions.

However, in numerical simulations the density contours are not smooth and are sensitive to the presence of small satelites. For this reason we choose to measure the shape by taking volume-enclosed particles, rather than shell-enclosed. We follow the shape measurement method presented by Allgood et al. (2006) that uses the reduced inertia tensor,

$$I_{ij} = \sum_k \frac{x_k^{(i)} x_k^{(j)}}{d_k^2}, \tag{1}$$

with the positions components weighted by the k-th particle distance $d_k^2 = x_k^2 + y_k^2 + z_k^2$, the particle positions are measured from the minimum of the gravitational potential in each halo. The diagonalization of this tensor yields the principal axes of the structure as well as the eigen-quantities which are proportional to the squared principal axes $a > b > c$.

We start the calculations taking into account particles within a sphere of radius R and then recharacterize the triaxial parameters by taking into account particles within

Halo	$N_P/10^6$		$M_P/10^5 M_\odot$		$R_{vir}/$kpc		$M_{vir}/10^{14} M_\odot$	
	DM	MHD	DM	MHD	DM	MHD	DM	MHD
halo 1	4.068	2.447	2.397	2.022	196.927	187.674	9.062	7.844
halo 2	5.625	5.457	2.481	2.093	235.094	233.934	15.418	15.191
halo 3	3.826	3.852	2.645	2.231	210.693	210.955	11.099	11.141
halo 4	4.585	4.530	2.590	2.185	219.378	215.438	12.529	11.866
halo 5	3.262	3.290	2.533	2.137	196.984	197.246	9.071	9.106
halo 6 ($\star$)	3.184	3.110	2.337	1.972	191.840	189.342	8.378	8.054
halo 7	3.878	3.729	2.296	1.937	197.864	196.509	9.193	9.005
halo 8	2.772	2.796	2.451	2.068	190.716	191.764	8.231	8.368
halo 9	3.038	3.010	2.738	2.310	195.826	190.640	8.911	8.222
halo 10	2.700	2.751	2.541	2.144	187.139	188.147	7.777	7.904
halo 11	4.146	4.116	2.541	2.144	221.821	219.568	12.952	12.560
halo 12	2.865	2.908	2.645	2.231	192.280	192.038	8.436	8.404
halo 13	3.520	3.600	2.393	2.019	202.139	203.815	9.801	10.048
halo 14	4.200	4.475	2.499	2.108	215.535	218.927	11.882	12.453
halo 15	2.888	2.845	2.541	2.144	199.848	200.658	9.471	9.588
halo 16 ($\star$)	3.821	3.871	2.499	2.108	212.590	212.632	11.401	11.408
halo 17	2.752	2.781	2.552	2.153	188.067	187.404	7.893	7.811
halo 18	3.770	3.624	2.738	2.310	201.124	207.293	9.655	10.571
halo 19	2.989	3.086	2.645	2.231	200.244	200.325	9.527	9.540
halo 20	3.903	3.822	2.481	2.093	210.097	211.423	11.005	11.214
halo 21 ($\star$)	4.105	4.075	2.640	2.227	219.527	219.823	12.555	12.604
halo 22	2.794	2.766	2.625	2.215	188.363	184.801	7.931	7.489
halo 23 ($\star$)	3.977	4.073	2.795	2.358	217.768	215.959	12.254	11.952
halo 24 ($\star$)	4.466	4.426	2.522	2.127	217.440	215.147	12.199	11.817
halo 25	2.902	2.806	2.645	2.231	199.922	198.299	9.482	9.254
halo 26	4.610	4.716	2.506	2.115	219.984	218.939	12.633	12.454
halo 27 ($\star$)	5.060	5.018	2.590	2.185	228.036	226.225	14.071	13.740
halo 28	4.184	4.276	2.645	2.231	216.979	217.997	12.121	12.294
halo 29	4.827	4.613	2.499	2.108	225.791	219.935	13.660	12.625
halo 30	3.268	3.112	2.579	2.176	195.043	194.741	8.805	8.763

Table 3. Specifications of each level 4 galaxy (halo). The DM and MHD versions of each parameters are presented together. The columns correspond to: (1) Halo name, (2,3) Millions of DM particles belonging to the halo, (4,5) DM particle mass in $10^5 M_\odot$, (6,7) Halo Virial radius in kpc and (8,9) halo virial mass in $10^{14} M_\odot$. Halos marked with a star ($\star$) are correspond to halos resimulated at higher resolution (level 3).

Halo	$N_P/10^6$		$M_P/10^5 M_\odot$		$R_{vir}/$kpc		$M_{vir}/10^{14} M_\odot$	
	DM	MHD	DM	MHD	DM	MHD	DM	MHD
halo 6	24.902	24.185	0.292	0.246	191.741	188.367	8.365	7.932
halo 16	29.750	30.334	0.312	0.263	212.622	212.542	11.406	11.395
halo 21	31.993	31.503	0.330	0.278	219.731	220.250	12.588	12.679
halo 23	31.379	31.618	0.349	0.295	217.793	213.358	12.259	11.524
halo 24	34.987	35.153	0.315	0.266	217.313	213.963	12.179	11.624
halo 27	39.617	39.056	0.324	0.273	227.908	223.484	14.048	13.244

Table 4. Same layout Table 4 for Level 3 simulations (higher resolution than Level 4 simulations).

an ellipsoid of semi-axes $r, r/q, r/s$ and re-scaled distance $d^2 = x^2 + (y/q)^2 + (z/s)^2$, where $q = b/a$ and $s = c/a$ are the previously calculated axial ratios. We repeat this process until the average deviation of semi-axes is less than 10^{-6}. This is the same method used to estimate the halo shape in the DM-only Aquarius simulations (Vera-Ciro et al. 2011).

We restrict the sampling of the ellipsoidal parameters to radii between $1/16 R_{vir}$ and $2 R_{vir}$, where R_{vir} is taken as the radius enclosing a sphere with 500 times the average dark matter density of the Universe. All our results use of this reference radius unless strictly stated otherwise. We peform the shape measurements both as a function of radius and redshift for all halos in the sample.

4 RESULTS

4.1 Radial trends at $z = 0$

We find that in DM-only simulations halos are monotonically rounder with increasing radius, confirming results already reported in the literature (Vera-Ciro et al. 2011). Figure 1 illustrates this effect. There we show the density a DM-only halo at redshift zero in a thin slice passing through the halo's centre, each panel shows the halo at different radii. The ellipse plotted over the contours indicates the outermost boundary of the estimated shape ellipsoid. Indeed, the ellipse panel on the right (outer halo) is rounder than the ellipse on the left (inner halo).

We quantify this effect by plotting the axial ratios q, s, s/q and the triaxiality $T \equiv \frac{1-q}{1-s}$ as a function of radius. As a

(a) halo 27 DM shape at small radius

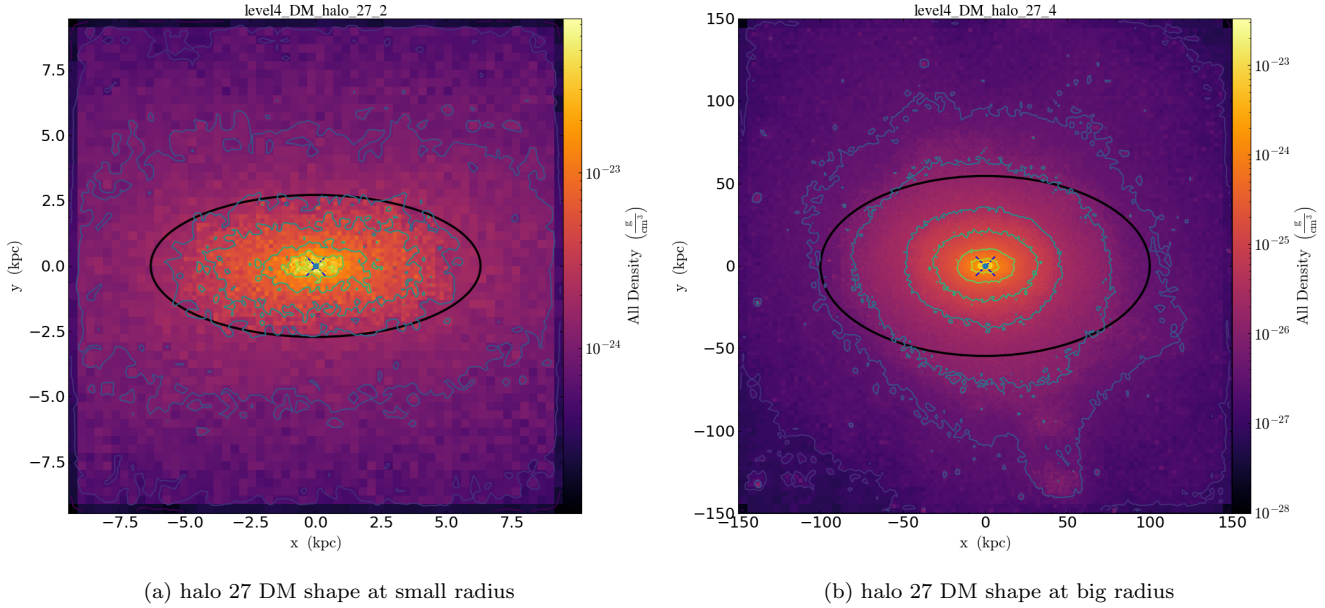(b) halo 27 DM shape at big radius

Figure 1. DM density for inner/outer (left/right panel) DM halo regions. Slice 20 percent of the max-min range in the "z" position of particles belonging to the main structure, centered at halo defined position (calculated with most bounded particle)

representative sample of this relations we show on Figure 2 the radial trends for Halo 16 at the highest resolution both for DM and MHD simulations. The continous lines correspond to the DM simulation and shows how the inner part of the halo $r \approx 1\,\mathrm{kpc}\,h^{-1}$ has values of $q = 0.5$, $s = 0.5$ while at the virial radius the same quantities increase to $q = 0.85$, $s = 0.6$; in turn the triaxiality decreases from $T \approx 1.0$ to $T \approx 0.4$.

In the same Figure 2 we also find one of the main results of our study: halos in MHD simulations are systematically rounder, at every radius, than its DM-only counterparts. The dashed line in Figure 2 shows that at $r \approx 1\,\mathrm{kpc}\,h^{-1}$ in the MHD simulation we have $q = 0.85$, $s = 0.8$ ($q = 0.5$, $s = 0.5$ in DM) and at the virial radius $q = 0.95$, $s = 0.75$ ($q = 0.85$, $s = 0.6$ in DM). However, the triaxiality trend is not as monotonous for MHD halos is it is in DM halos. The triaxiality goes almost to zero at an intermediate radius, $r \approx 10\,\mathrm{kpc}$ in the case of Halo 16 in Figure 2, to increase again. **pasa lo mismo para todos los halos? es lo mismo para baja y alta resolucion de MHD?**

Figure 3 summarizes this comparizon for all 30 halos in the Level 3 simulations. Measurements at $R_{\mathrm{vir}}/16$ are represented by circlse while squares are measurements at R_{vir}. All halos, except two, show that outer regions rounder than inner regions. The exceptions are cases where a merging substructures near the halo's center give rise to perturbed axial ratios measurments. Figure **??** shows the same information, this time for the MHD simulations. The main radial trend continues to hold, albet less pronounced; halos in MHD simulations are in general rounder than their DM counterparts and the increased roundness in outer regions is less pronounced on average.

This situation is summarized Table **??** We summarize these resulta in Table **??**

Concerning MHD halos, *prescindible?(((the expected tendency is not clear. Some studies claim that the DM halo*

	$R_{1/16}$	$R_{1/8}$	$R_{1/4}$	$R_{1/2}$	R_1	R_2
$\bar{q}$	$0.55^{+0.07}_{-0.07}$	$0.57^{+0.09}_{-0.08}$	$0.61^{+0.15}_{-0.08}$	$0.65^{+0.18}_{-0.10}$	$0.70^{+0.13}_{-0.10}$	$0.75^{+0.10}_{-0.10}$
$\bar{s}$	$0.42^{+0.12}_{-0.03}$	$0.45^{+0.11}_{-0.04}$	$0.49^{+0.09}_{-0.05}$	$0.52^{+0.10}_{-0.05}$	$0.56^{+0.10}_{-0.05}$	$0.59^{+0.11}_{-0.06}$
$\bar{T}$	$0.89^{+0.03}_{-0.08}$	$0.88^{+0.04}_{-0.12}$	$0.84^{+0.08}_{-0.23}$	$0.81^{+0.08}_{-0.29}$	$0.75^{+0.14}_{-0.25}$	$0.71^{+0.16}_{-0.19}$

Table 5. Median values of axial ratios q, s and triaxiality parameter T for DM halos in DM-only simulations at different radii (columns).

	$R_{1/16}$	$R_{1/8}$	$R_{1/4}$	$R_{1/2}$	R_1	R_2
$\bar{q}$	$0.93^{+0.04}_{-0.04}$	$0.95^{+0.03}_{-0.03}$	$0.95^{+0.02}_{-0.05}$	$0.93^{+0.04}_{-0.06}$	$0.93^{+0.04}_{-0.10}$	$0.92^{+0.03}_{-0.09}$
$\bar{s}$	$0.73^{+0.05}_{-0.09}$	$0.73^{+0.07}_{-0.10}$	$0.73^{+0.08}_{-0.10}$	$0.73^{+0.09}_{-0.08}$	$0.75^{+0.07}_{-0.11}$	$0.74^{+0.07}_{-0.10}$
$\bar{T}$	$0.31^{+0.15}_{-0.22}$	$0.20^{+0.24}_{-0.12}$	$0.24^{+0.20}_{-0.12}$	$0.30^{+0.26}_{-0.16}$	$0.36^{+0.23}_{-0.23}$	$0.39^{+0.26}_{-0.13}$

Table 6. Median values of axial ratios q, s and triaxiality parameter T for DM halos in MHD simulations at different radii (columns).

must be oblate, at least in the vicinities of the disk, to ensure its stability . However,))) not much is said about its dependence with radius as previous studies focus rather on the effects of baryons on the dynamics of the halo at fixed radii. Examining the representative behaviour of a MHD halo on figure **??**, some things are noticeable: first, the DM halo is almost perfectly oblate around $\approx 10 - 30kpc$, second, its axial ratio b/a start decreasing very slowly after $50kpc$ and below $10kpc$ and third, its axial ratio c/a does not exhibit noticeable change in the whole radial domain. (Pass from representative case to averaged values) These results are statistically supported and sumarized on table **??** and figure **??**
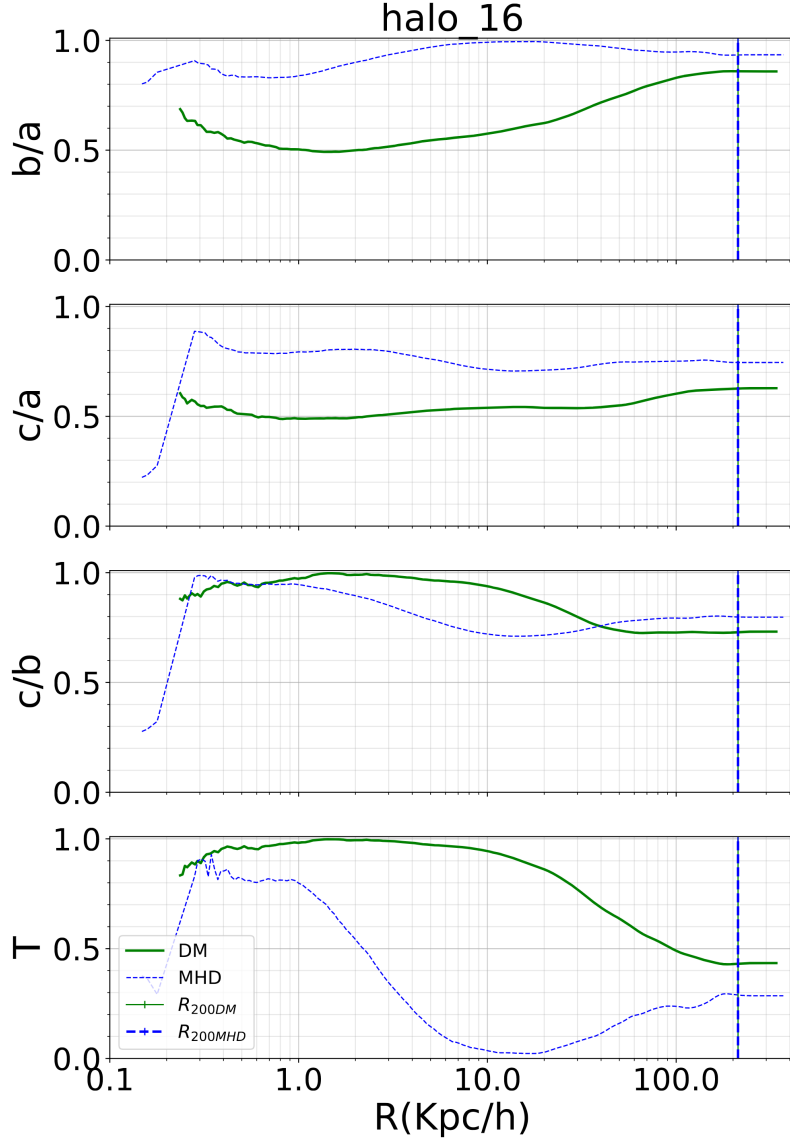
Figure 2. Radial profile for the axial ratios and the triaxiality parameter $T = \frac{1-b/a}{1-c/a}$ at redshift $z = 0$. Radial profile was sampled at redshift 0 and there are two sets of lines showing MHD and DM-only versions of the axial ratios profile

4.2 Comparison with observational constraints

To be able to compare our results with observational values, we must relate the calculated quanties with their corresponding isopotential analogue, in which observational constraints are usually presented. For this purpose, we run a simple algorithm to find an approximation of the shape of the isopotential contour. Here, we calculate the mean and standard deviation of the potential over a spherical shell of width equals to 10% of the radius at which it is sampled. Then, we calculate the inertia tensor of particles with potential within 1σ around the mean potential and calculate its triaxial characterization with the reduced inertia tensor. We repeat the process of calculating the potential mean and standard deviation until convergence is achieved with tolerance of 10^{-4}. We repeat this process for the different radii from table 7.

	$R_{1/8}$	$R_{1/4}$	$R_{1/2}$	R_1
$\bar{q}$	$0.98^{+0.01}_{-0.02}$	$0.97^{+0.01}_{-0.04}$	$0.96^{+0.03}_{-0.06}$	$0.94^{+0.03}_{-0.07}$
$\bar{s}$	$0.89^{+0.04}_{-0.06}$	$0.88^{+0.04}_{-0.04}$	$0.87^{+0.05}_{-0.05}$	$0.85^{+0.05}_{-0.05}$
$\bar{T}$	$0.18^{+0.23}_{-0.10}$	$0.36^{+0.19}_{-0.21}$	$0.40^{+0.26}_{-0.20}$	$0.48^{+0.23}_{-0.21}$

Table 7. Median values of isopotential axial ratios q, s and triaxiality parameter T for DM halos in MHD simulations at different radii (columns).

As a check of consistency, we compare our new isopotential shape results with the analytic expression of the $(1 - q_\phi)\frac{1}{3}(1 - q_\rho)$ (Binney & Tremaine 2008), taking the volume-enclosed axial ratios as an approximation for the isodensity contour ratios q_ρ. Although this analytic expression if meant to be used for logarithmic axisymmetric halos, it works well as a first approximation for nearly axisymmetric halos as those produced by our disced galaxies. We find that
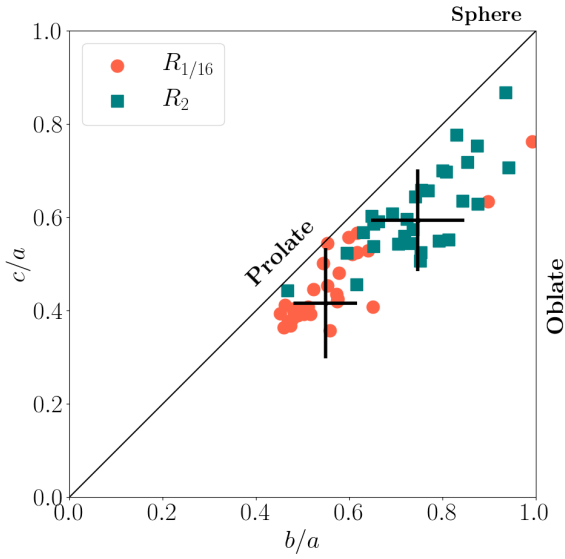
Figure 3. Axial ratios for the 30 halos in the Level 3 DM simulations. Each dot represents the shape characterization of each halo at the 2 times the virial radius and a 1/16 fraction of the virial radius differentiated by color. Errorbar shows median and errors for each sampled radii. Conclusion: DM halos are rounder on the outskirts **Esto necesita correccion. Debe ser a R1/16 y R (no 2R!)**
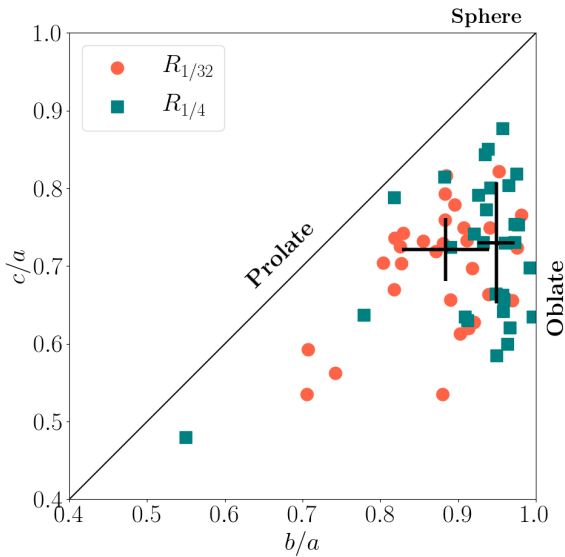

Figure 4. Axial ratios for the 30 halos in the Level 3 MHD simulations. DM halos are rounder at larger radii than small radii. **Esto necesita correccion para que tambien sea a R1/16 y R.**

the difference between the real and the analytic isopotential axial ratios is not bigger than *quantitypercent*. With this, we may now present on table 7 our observationally-comparable results for MHD halos at two important radii one corresponding to the approximate regimes where the MW DM halo is usually constrained.

Little discussion: Are our results congruent with observations? at which radii, does the DM halo shape vary that much?. Which models are favored?
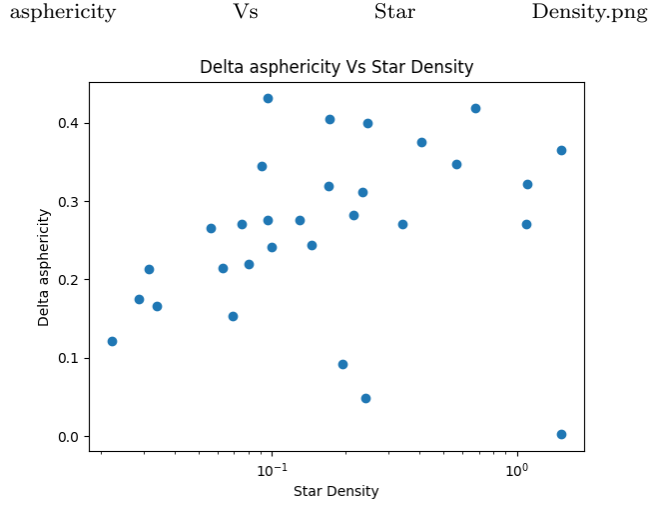
Figure 5. Difference in asphericities between MHD and DM shapes Vs Star Density of the simulation. Unsure about this graphic. Take delta asphericity as the strength of the rounding effect of baryons.

4.3 The rounding effect of baryons

From the previous characterization of radial shapes it is clear that MHD halos are rounder than DM halos (i.e. axial ratios are bigger) at every sampled radii. This can be compared on tables 5 and 6 or at the representative example on figure **??**. From there, it is also noticeable that the rounding effect of baryons is stronger at the disk regime, where the DM halo is almost perfectly oblate. Furthermore, MHD halos tend towards more oblate shapes (T < 0.5) despite DM halos tendency towards more prolate shapes (T>0.5).

This rounding effect is expected from the gravitational effect of the flattened axisymmetric galactic disk. It is also reasonable that this effect is not as strong at $\approx$ 100kpc, where the disk potential is dimmer compared to the DM halo potential. Keeping this in mind, one would expect that the rounding effect of baryons is related to some galactic parameters such as its component masses and radii. However, even for the parameter of highest correlation with this rounding effect (the baryonic fraction), the relation is not clear nor conclusive due to the dispersion from galaxy peculiarities. In figure 5 we plot the ratios c/a compared to the baryonic fraction of each galaxy. Although some linear tendency is suggested qualitatively, the dispersion of the sample is very high to obtain some conclusive relation. This is an evidence that adiabatic-contraction models are not realistic as they may neglect some effects of the galaxy evolution in the whole cosmological context.

Actually we have not examined the relation of c/a in MHD halos with some measure of c/a from the disk, that is something like Zdisk/Rdisk. This actually would make more sense from a physical point of view: effect of the potential.

Although the effect of the baryonic disk on the shape of the DM halo is a reasonable explanation for the rounding effect, it does not actually explain the deviation from oblateness of MHD halos at $r < 10$kpc. In other words, if the disk
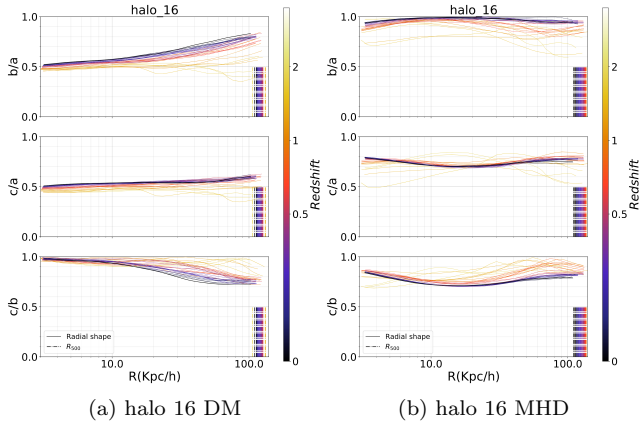
(a) halo 16 DM   (b) halo 16 MHD

Figure 6. Radial profile (comoving) of axial ratios for halo 16 in terms of redshift (color). This halo maintains its shape until $z \approx 1$ obviating the systematic rounding effect in time from asymmetric potentials. Each plot-line represents the radial profile at a determined redshift. Conclusion: Mainly for b/a, it increases for: (1) for bigger radii (fixed redshift)(2) for lower redshift (fixed radius) It explains the correlation between radial profile and history, but does not require that curves match in the triaxial plane.

is perfectly axisymmetric, there must be some source of triaxiality at $r < 10$kpc to explain the low axial ratios.

Talk about source of triaxiality at the inner parts of the halos (bar?). This source of triaxiality at the inner parts explains why the axial ratios are ≈ 0.95 and not exactly 1. We should also discuss that the decrease in the axial ratios for bigger radii may actually be bigger/steeper but it is dimmed by the contribution of inner parts.

4.4 The historical shape

One of the principal motivations to study the radial dependence of the DM halo shape is that it may encode some clues about its formation history. We have already shown that DM-only halos seem to exhibit a steady and monotonous growth in its axial ratios when sampled at bigger radii. One similar effect can be found if we sample the shape at the virial radius, this time at varying redshift. It is easy to see that the axial ratios increase with decreasing redshift, which is expected by the continuous influence of the gravitational potential Vera-Ciro et al. (2011). In figure 6 we present a representative example.

Interestingly, these two parametic plots i.e. $(b/a, c/a)(z = 0, r)$ and $(b/a, c/a)(z, r = R_{vir})$ are very correlated for DM-only halos 7. This means that, for DM-only halos, one can approximate its shape at higher redshift by simply sampling its current shape at a smaller radius **wording**. This relationship relies strongly on the steady and monotonous tendency of DM halos towards sphericity for bigger radii and smaller redshift.

MHD halos, on the other hand, do not exhibit tendency towards sphericity with bigger radii, but they do get sistematically rounder at lower redshift as seen in figure 6. This effectively vanishes this correlation as seen from a DM halo 8.
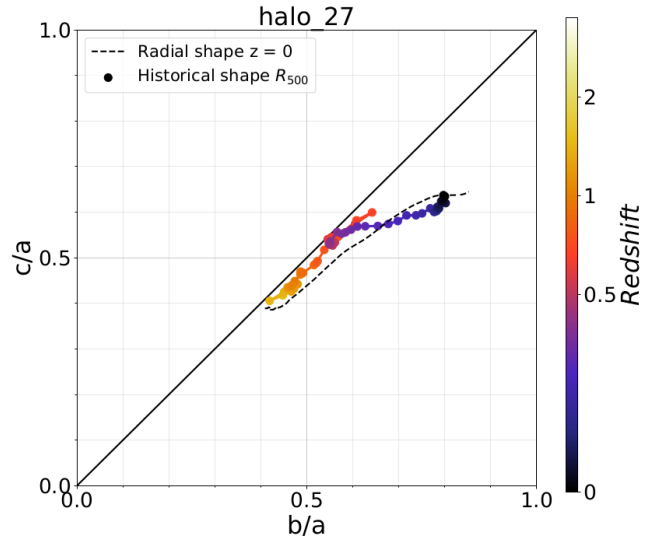
Better graphics.

Figure 7. DM only Radial profile at redshift 0 (dashed line) Historical profile at virial radius R500 (colour line). Example of a halo where there is some correlation between these two profiles, as usually happens for DM only simulations. Conclusion: DM only halos usually (fraction?) have correlated shape profiles.
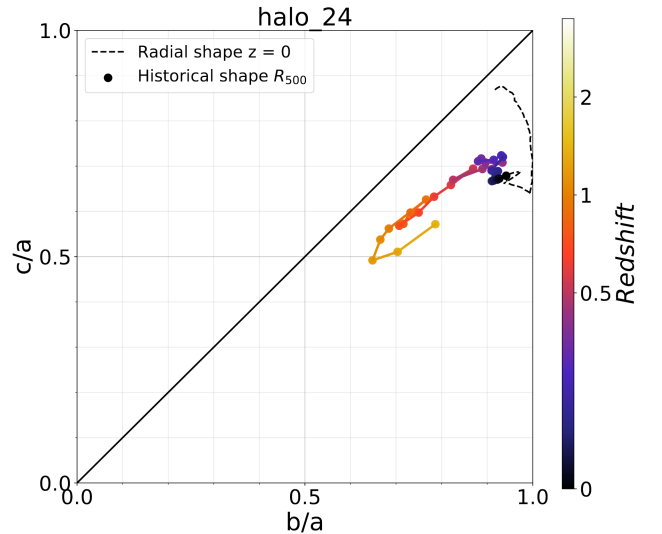

Figure 8. MHD. Radial profile at redshift 0 (dashed line) Historical profile at virial radius R500 (colour line) Example of a halo where there is no correlation between these two profiles, as usually happens in MHD. Conclusion: MHD halos usually (fraction?) have uncorrelated shape profiles.

4.5 The orientation of the principa axes

One of the principal assumptions of observational models of the MW's DM halo is that its minor axis is perfectly aligned with the disk axis. Although this is a reasonable assumption to guarantee the stability of the galactic disk in simplified models of isolated galaxies, it may not be the case for galaxies evolved in the whole cosmological context nor at every radii at which the shape is sampled.

Therefore, it is of special interest to us to examin the

strength of this alignment assumption in the context of simulations. For this purpose, we sampled the shape at 5 different radii and plotted the axial directions, as well as the disk direction in the **name** diagrams (explain diagrams). Explain disk direction calculation.

We found that there is not a representative example of what happens in terms of alignments. We found that the majority of the disks are aligned with the minor axis of their DM halo within $\approx 30^o$; in some special cases, this alignment was almost perfect and in some other cases, the DM halo minor axis changed substantially to be able to determine an alignment. In figure 9 we present these three cases. **occurrencies for each case?**

This is an important result of our study. We study the radial evolution of the principal axes, compared also to the angular momentum vector from the disk. We found that while the angular momentum tend to be aligned with the minor axis of the ellipsoid, this may not be the case all times. When there is an alignment it is usually within 20 degrees (get a histogram of this. and an evolution of this histogram with time). When there is not an alignment, then there is no simple way to determine towards which axis it is oriented. Furthermore, the principal axes alignment usually change with radius (rotation, swap, verify). This ask for relaxation on the strong constrains on the MW DM halo models.

Discussion about the distribution of alignments and their evolution in time: Precesion or temporary instabilities?

5   CONCLUSIONS

6   DISCUSSION

ACKNOWLEDGEMENTS

REFERENCES

Abadi M. G., Navarro J. F., Fardal M., Babul A., Steinmetz M., 2010, MNRAS, 407, 435

Allgood B., Flores R. A., Primack J. R., Kravtsov A. V., Wechsler R. H., Faltenbacher A., Bullock J. S., 2006, MNRAS, 367, 1781

Banerjee A., Jog C. J., 2011, ApJ, 732, L8

Binney J., Tremaine S., 2008, Galactic Dynamics: Second Edition. Princeton University Press

Bovy J., Bahmanyar A., Fritz T. K., Kallivayalil N., 2016, ApJ, 833, 31

Bowden A., Evans N. W., Williams A. A., 2016, MNRAS, 460, 329

Bryan S. E., Kay S. T., Duffy A. R., Schaye J., Dalla Vecchia C., Booth C. M., 2013, MNRAS, 429, 3316

Chua K. E., Pillepich A., Vogelsberger M., Hernquist L., 2018a, preprint, (arXiv:1809.07255)

Chua K. E., Pillepich A., Vogelsberger M., Hernquist L., 2018b, preprint, (arXiv:1809.07255)

Debattista V. P., Moore B., Quinn T., Kazantzidis S., Maas R., Mayer L., Read J., Stadel J., 2008, The Astrophysical Journal, 681, 1076

(a) Perfectly aligned Axes

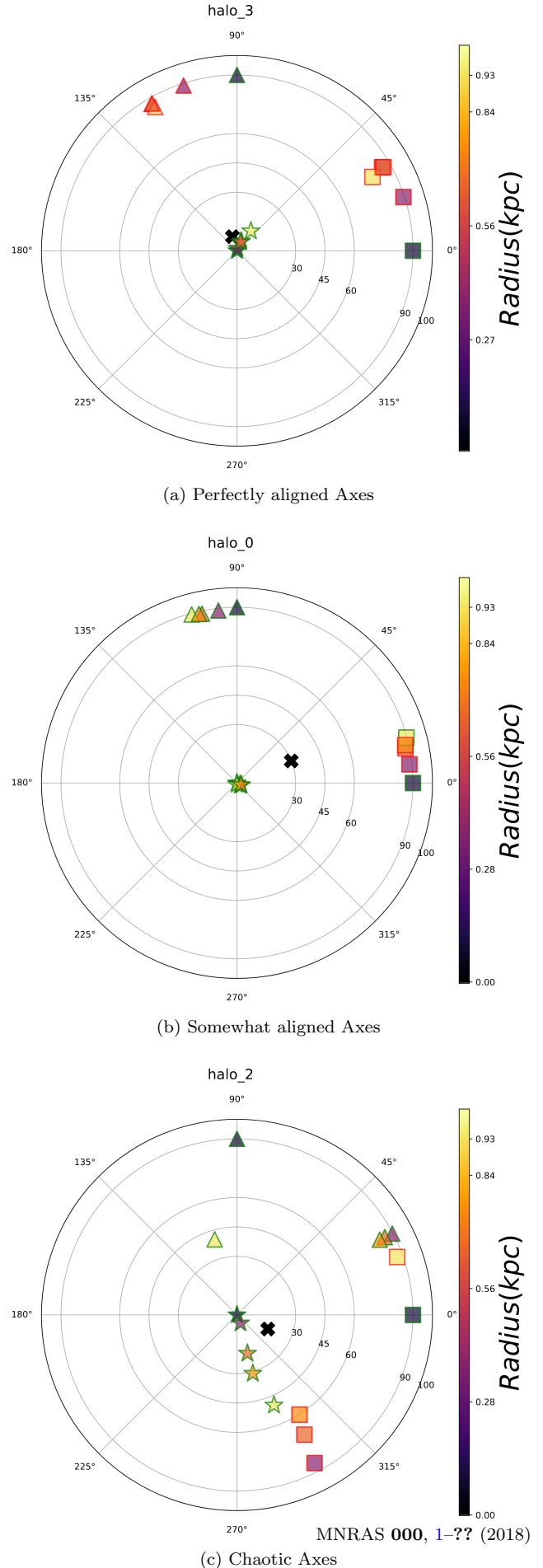(b) Somewhat aligned Axes

(c) Chaotic Axes

Figure 9. Star: Minor Axis Triangle: Medium Axis Square: Major Axis Color: Radii at which shape was sampled (show radii

Debattista V. P., Roškar R., Valluri M., Quinn T., Moore B., Wadsley J., 2013, MNRAS, 434, 2971

Deg N., Widrow L., 2013, MNRAS, 428, 912

Grand R. J. J., et al., 2017, Monthly Notices of the Royal Astronomical Society, 467, 179

Ibata R., Lewis G. F., Martin N. F., Bellazzini M., Correnti M., 2013, ApJ, 765, L15

Johnston K. V., Law D. R., Majewski S. R., 2005, ApJ, 619, 800

Kazantzidis S., Abadi M. G., Navarro J. F., 2010, ApJ, 720, L62

Law D. R., Majewski S. R., 2010, The Astrophysics Journal, 714, 229

Law D. R., Majewski S. R., Johnston K. V., 2009, The Astrophysical Journal Letters, 703, L67

Loebman S. R., Ivezić Ž., Quinn T. R., Governato F., Brooks A. M., Christensen C. R., Jurić M., 2012, ApJ, 758, L23

Olling R. P., Merrifield M. R., 2000, MNRAS, 311, 361

Pearson S., Küpper A. H. W., Johnston K. V., Price-Whelan A. M., 2015, ApJ, 799, 28

Schaye J., et al., 2015, Monthly Notices of the Royal Astronomical Society, 446, 521

Springel V., 2010, Monthly Notices of the Royal Astronomical Society, 401, 791

Vera-Ciro C., Helmi A., 2013, ApJ, 773, L4

Vera-Ciro C. A., Sales L. V., Helmi A., Frenk C. S., Navarro J. F., Springel V., Vogelsberger M., White S. D. M., 2011, MNRAS, 416, 1377